CHEMISTRY
A EUROPEAN JOURNAL

DOI: 10.1002/chem.200701449

Homochiral Laminar Europium Metal–Organic Framework with Unprecedented Giant Dielectric Anisotropy

Zhi-Rong Qu,[a] Qiong Ye,[a] Hong Zhao,[a] Da-Wei Fu,[a] Heng-Yun Ye,[a] Ren-Gen Xiong,*[a] Tomoyuki Akutagawa,*[b] and Takayoshi Nakamura[b]

Abstract: Hydrothermal (deuteratothermal) reaction of L-ethyl lactate (Lig-Et) with $Eu(ClO_4)_3{\cdot}6H_2O$ gives colorless block crystals of $[Eu(Lig)_2(X_2O)_2][ClO_4]$ (**1**, X = H; **2**, X = D) both of which possess a two-dimensional laminar homochiral framework. Single-crystal dielectric measurements reveal that **1** and **2** display a giant dielectric anisotropy approximately exceeding 100 and large isotopic effect with about 54% enhancement along the *a* axis. Their ferroelectric features further confirm this respect. Crystal parameters: **1**, $C_6H_{14}ClO_{12}Eu$, M_r = 465.58, monoclinic, C_2, a = 8.6786(6), b = 8.3965(6), c = 10.2153(7) Å, β = 92.040(1)°, V = 743.92(9) Å^3, Z = 2, ρ_{calcd} = 2.079 Mg m^{-3}, R_1 = 0.0508, wR_2 = 0.1239, μ = 4.448 mm^{-1}, S = 1.043; Flack = 0.04(5). **2**: $C_6H_{10}D_4ClO_{12}Eu$, M_r = 469.61, monoclinic, C_2, a = 8.689(2), b = 8.410(2), c = 10.224(3) Å, β = 92.057(4)°, V = 746.7(3) Å^3, Z = 2, ρ_{calcd} = 2.089 Mg m^{-3}, R_1 = 0.0465, wR_2 = 0.1150, μ = 4.432 mm^{-1}, S = 1.058; Flack = 0.02(5).

Keywords: dielectric anisotropy · europium · organic–inorganic hybrid composites · structure elucidation

Introduction

The relative dielectric constant ε_r varies little with anisotropy, with the largest known anisotropic ratio approaching a value less than 10^2 and which either sharply drops to 1–2 orders of magnitude or almost vanishes between two different directions with increasing phase-transition temperature. In contrast, conductivity is a strong function of direction and the best known example of this is the large anisotropic ratio [$\delta\parallel$ (= 222700 S cm^{-1})/$\delta\perp$ (= 0.22 S cm^{-1})] of electric conductivity of a layered graphite monocrystal exceeding 10^5.[1] Consequently, it has remained a significant challenge to develop large dielectric anisotropy (defined as $\Delta\varepsilon = \varepsilon_{\parallel} - \varepsilon_{\perp}$ or $\Phi\varepsilon = \varepsilon_{\parallel}/\varepsilon_{\perp}$, in which $\varepsilon_{\parallel}$ or $\varepsilon_{\perp}$ is the real part of the complex permittivity $\varepsilon = \varepsilon_r + i\varepsilon_a$, and one of the most important physical properties of liquid crystalline compounds that in essence determine the lower threshold voltage of liquid crystal displays (LCDs).[2] Evidently, from a structural point of view, the anisotropic nature of a laminar structure may be largest between the parallel and perpendicular directions to the layer. Thus, a way to introduce high dielectric anisotropy is the design of layered compounds. Another consideration is that dielectric permittivity magnitude is also strongly dependent on molecular polarity. That is to say that a compound with a noncentrosymmetric structure will display large dielectric constant which can be $\gg 1000+$ probably due to their residual dipole moments resulting from an acentric packing mode.[3] It could thus be envisioned that the combination of both features would lead to new dielectric properties. To this end and as a continuation of systematic investigations in our group on optoelectronic properties of non-centrosymmetric compounds,[4] we have realized two homochiral europium compounds possessing residual dipole moments that lead to large ε_r and in principle in which the layered structures may display large $\Phi\varepsilon$ in accordance to the above-mentioned criteria.[4c]

[a] Dr. Z.-R. Qu, Dr. Q. Ye, Dr. H. Zhao, Dr. D.-W. Fu, Dr. H.-Y. Ye, Prof. Dr. R.-G. Xiong
Ordered Matter Science Research Center
Southeast University, Nanjing, 210096 (P. R. China)
Fax: (+86) 25-5209-0626
E-mail: xiongrg@seu.edu.cn

[b] Prof. Dr. T. Akutagawa, Prof. Dr. T. Nakamura
Research Institute for Electronic Science
Hokkaido University, Sapporo 060–0812 (Japan)
Fax: (+81) 11-706-4972
E-mail: takuta@imd.es.hokudai.ac.jp

Supporting information for this article is available on the WWW under http://www.chemeurj.org/ or from the author.

Results and Discussion

Hydrothermal or deuteratothermal reaction of $Eu(ClO_4)_3{\cdot}6H_2O$ with L-ethyl lactate (Lig-Et) gave the laminar

homochiral metal–organic frameworks (MOFs) $[Eu(Lig)_2(H_2O)_2][ClO_4]$ (**1**) and $[Eu(Lig)_2(D_2O)_2][ClO_4]$ (**2**), respectively (Scheme 1), in which $\Phi\varepsilon$ in both **1** and **2** are $\geqslant 100+$ and are stable during the measurement temperature range which is unprecedented.

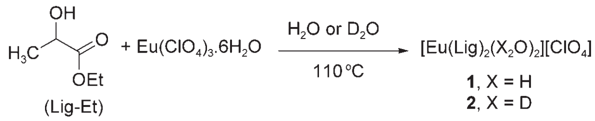

Scheme 1.

The IR spectrum of MOF **1** reveals a very strong peak at 1105 cm^{-1}, which suggests the presence of the ClO_4^- ion. The presence of three strong peaks at 1604, 1470, and 1434 cm^{-1} is also suggestive of the carboxylate moiety. As expected, a broad peak at 3480 cm^{-1} indicates the presence of water in **1**. The peaks in the IR spectrum of **2** are similar to those of **1**, but with the exception of an extra medium strong peak at 2515 cm^{-1}, indicating the presence of deuterated water.

X-ray crystal structure determination of MOFs **1** and **2** reveal that the local coordination environment around the Eu ion displays a slightly distorted square antiprism or dodecahedron with six oxygen atoms from four different lactate ions and two H_2O molecules (or D_2O) completing the eight-coordination mode.[5] Thus, each lactate ion links two Eu ions through one of the two oxygen atoms of the carboxylate moiety and the hydroxyl group that chelates a Eu ion with the other oxygen atom of the carboxylate group bridging to another Eu ion. This results in the formation of two-dimensional layered framework as depicted in Figure 1 (top right). Careful inspection of Figure 1 (bottom right) shows that a cation laminar layer of $[Eu(Lig)_2(X_2O)_2]^+$ (X=H or D) acts as the sides of a sandwich to intercalate perchlorate ions, resulting in the formation 3D framework through hydrogen bonds (see the Supporting Information). As expected, the dielectric constants parallel to the $[Eu(Lig)_2(X_2O)_2]^+$ (X=H or D) layer may be quite different from that perpendicular it. Also, there is nothing exceptional about their bond lengths and angles (Tables 1 and 2) found in **1** and **2**.

The temperature dependence of the ac dielectric permittivity measurements on an impedance analyzer on single crystals of **1** and **2** were carried out over the 5–300 K temperature range and at 10^6 Hz frequency. Electrical contacts were prepared by using gold paste to attach the 10 μm gold wires to the single crystal. As shown in Figure 2, the permittivity ε_{ra} of a single crystal of **1** along the *a* axis ($E \| a$, electric field (E) approximately parallel to *a* axis) reveals that the dielectric permittivity remains unchanged over the 5–300 K temperature range at a high frequency of 1 MHz, and maintains a value range of $\varepsilon_{ra}(\mathbf{1}) \approx 14.3$–15.4. Surprisingly,

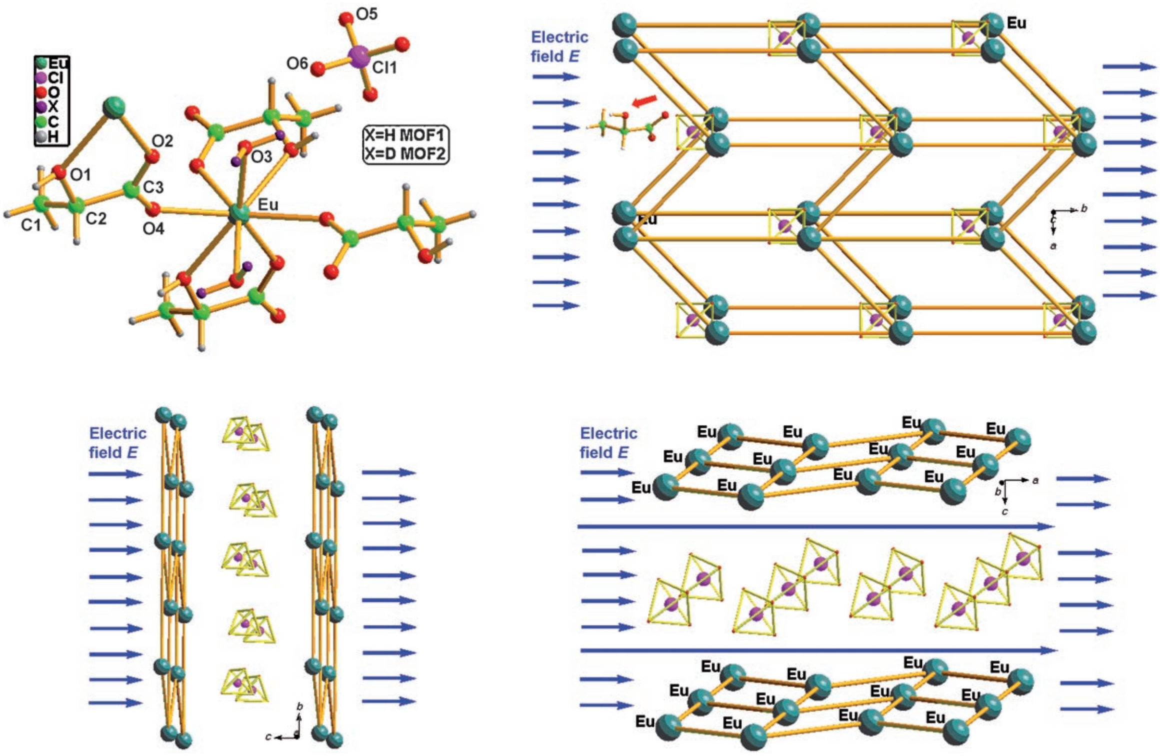

Figure 1. Top left: Asymmetric unit of MOF **1** and **2** in which Eu anion has an eight-coordinate local coordination geometry. Top right: two-dimensional laminar framework of **1** and **2** along the *c* axis in which the ClO_4^- ions are intercalated between two layers and long orange sticks and grey-green balls stand for L-lactate and Eu atoms. Bottom left: two-dimensional layered representation of **1** and **2** along the *a* axis. Bottom right: two-dimensional layered representation of **1** and **2** along the *b* axis. The blue arrows indicate the electric field directions.

Table 1. Bond lengths [Å] and angles [°] for MOF **1**.[a]

C1−C2	1.51(3)	C2−O1	1.37(2)
C2−C3	1.48(2)	C3−O4	1.18(2)
C3−O2	1.279(19)	Cl1−O5$^{\#1}$	1.267(10)
Cl1−O5	1.267(10)	Cl1−O6	1.273(13)
Cl1−O6$^{\#1}$	1.273(12)	Eu1−O2$^{\#2}$	2.303(11)
Eu1−O2$^{\#3}$	2.303(11)	Eu1−O3$^{\#4}$	2.389(10)
Eu1−O3	2.389(10)	Eu1−O4	2.424(11)
Eu1−O4$^{\#4}$	2.424(11)	Eu1−O1$^{\#3}$	2.456(11)
Eu1−O1$^{\#2}$	2.456(11)	O1−Eu1$^{\#5}$	2.456(11)
O2−Eu1$^{\#5}$	2.303(11)		
O1-C2-C3	108.6(15)	O1-C2-C1	112.7(13)
C3-C2-C1	110.4(14)	O4-C3-O2	123.4(15)
O4-C3-C2	122.2(15)	O2-C3-C2	114.5(15)
O5$^{\#1}$-Cl1-O5	103.2(10)	O5$^{\#1}$-Cl1-O6	106.6(7)
O5-Cl1-O6	109.3(8)	O5$^{\#1}$-Cl1-O6$^{\#1}$	109.3(8)
O5-Cl1-O6$^{\#1}$	106.6(7)	O6-Cl1-O6$^{\#1}$	120.6(13)
O2$^{\#2}$-Eu1-O2$^{\#3}$	88.4(8)	O2$^{\#2}$-Eu1-O3$^{\#4}$	97.5(5)
O2$^{\#3}$-Eu1-O3$^{\#4}$	149.4(4)	O2$^{\#2}$-Eu1-O3	149.4(4)
O2$^{\#3}$-Eu1-O3	97.5(5)	O3$^{\#4}$-Eu1-O3	92.5(5)
O2$^{\#2}$-Eu1-O4	133.6(4)	O2$^{\#3}$-Eu1-O4	78.9(4)
O3$^{\#4}$-Eu1-O4	75.3(4)	O3-Eu1-O4	76.9(4)
O2$^{\#2}$-Eu1-O4$^{\#4}$	78.9(4)	O2$^{\#3}$-Eu1-O4$^{\#4}$	133.6(4)
O3$^{\#4}$-Eu1-O4$^{\#4}$	76.9(4)	O3-Eu1-O4$^{\#4}$	75.3(4)
O4-Eu1-O4$^{\#4}$	139.4(5)	O2$^{\#2}$-Eu1-O1$^{\#3}$	78.6(5)
O2$^{\#3}$-Eu1-O1$^{\#3}$	62.1(4)	O3$^{\#4}$-Eu1-O1$^{\#3}$	148.6(4)
O3-Eu1-O1$^{\#3}$	77.9(5)	O4-Eu1-O1$^{\#3}$	129.5(4)
O4$^{\#4}$-Eu1-O1$^{\#3}$	71.7(4)	O2$^{\#2}$-Eu1-O1$^{\#2}$	62.1(4)
O2$^{\#3}$-Eu1-O1$^{\#2}$	78.6(5)	O3$^{\#4}$-Eu1-O1$^{\#2}$	77.9(5)
O3-Eu1-O1$^{\#2}$	148.6(4)	O4-Eu1-O1$^{\#2}$	71.7(4)
O4$^{\#4}$-Eu1-O1$^{\#2}$	129.5(4)	O1$^{\#3}$-Eu1-O1$^{\#2}$	124.6(7)
C2-O1-Eu1$^{\#5}$	123.8(10)	C3-O4-Eu1	139.6(10)

[a] Symmetry transformations used to generate equivalent atoms: #1 $-x+2$, y, $-z+1$; #2 $x+1/2$, $y+1/2$, z; #3 $-x+3/2$, $y+1/2$, $-z+2$; #4; $-x+2$, y, $-z+2$; #5 $x-1/2$, $y-1/2$, z.

Table 2. Bond lengths [Å] and angles [°] for MOF **2**.[a]

C1−C2	1.50(2)	C2−O1	1.406(19)
C2−C3	1.48(2)	C3−O4	1.207(19)
C3−O2	1.282(17)	Cl1−O6	1.296(11)
Cl1−O6$^{\#1}$	1.296(11)	Cl1−O5	1.299(11)
Cl1−O5$^{\#1}$	1.299(11)	Eu1−O2$^{\#2}$	2.334(10)
Eu1−O2$^{\#3}$	2.334(10)	Eu1−O3	2.385(10)
Eu1−O3$^{\#4}$	2.385(10)	Eu1−O4	2.420(10)
Eu1−O4$^{\#4}$	2.420(10)	Eu1−O1$^{\#3}$	2.451(10)
Eu1−O1$^{\#2}$	2.451(10)	O1−Eu1$^{\#5}$	2.451(9)
O2−Eu1$^{\#5}$	2.334(10)	O3−D3 A	0.9377
O3−D3B	0.9732		
O1-C2-C3	107.3(11)	O1-C2-C1	112.9(12)
C3-C2-C1	111.3(13)	O4-C3-O2	122.2(14)
O4-C3-C2	120.2(13)	O2-C3-C2	117.6(14)
O6-Cl1-O6$^{\#1}$	120.5(12)	O6-Cl1-O5	108.0(7)
O6$^{\#1}$-Cl1-O5	108.3(6)	O6-Cl1-O5$^{\#1}$	108.3(6)
O6$^{\#1}$-Cl1-O5$^{\#1}$	108.0(7)	O5-Cl1-O5$^{\#1}$	102.3(11)
O2$^{\#2}$-Eu1-O2$^{\#3}$	87.9(6)	O2$^{\#2}$-Eu1-O3	148.8(4)
O2$^{\#3}$-Eu1-O3	98.3(4)	O2$^{\#2}$-Eu1-O3$^{\#4}$	98.3(4)
O2$^{\#3}$-Eu1-O3$^{\#4}$	148.8(4)	O3-Eu1-O3$^{\#4}$	92.0(5)
O2$^{\#2}$-Eu1-O4	133.9(3)	O2$^{\#3}$-Eu1-O4	78.5(4)
O3-Eu1-O4	77.2(3)	O3$^{\#4}$-Eu1-O4	75.2(4)
O2$^{\#2}$-Eu1-O4$^{\#4}$	78.5(4)	O2$^{\#3}$-Eu1-O4$^{\#4}$	133.9(3)
O3-Eu1-O4$^{\#4}$	75.2(4)	O3$^{\#4}$-Eu1-O4$^{\#4}$	77.2(3)
O4-Eu1-O4$^{\#4}$	139.9(5)	O2$^{\#2}$-Eu1-O1$^{\#3}$	77.5(4)
O2$^{\#3}$-Eu1-O1$^{\#3}$	63.2(3)	O3-Eu1-O1$^{\#3}$	78.2(4)
O3$^{\#4}$-Eu1-O1$^{\#3}$	148.0(3)	O4-Eu1-O1$^{\#3}$	130.2(3)
O4$^{\#4}$-Eu1-O1$^{\#3}$	70.9(3)	O2$^{\#2}$-Eu1-O1$^{\#2}$	63.2(3)
O2$^{\#3}$-Eu1-O1$^{\#2}$	77.5(4)	O3-Eu1-O1$^{\#2}$	148.0(3)
O3$^{\#4}$-Eu1-O1$^{\#2}$	78.2(4)	O4-Eu1-O1$^{\#2}$	70.9(3)
O4$^{\#4}$-Eu1-O1$^{\#2}$	130.2(3)	O1$^{\#3}$-Eu1-O1$^{\#2}$	124.8(6)
C2-O1-Eu1$^{\#5}$	123.9(7)	C3-O2-Eu1$^{\#5}$	127.5(10)
Eu1-O3-D3 A	111.4	Eu1-O3-D3B	109.5
D3 A-O3-D3B	110.2	C3-O4-Eu1	138.5(10)

[a] Symmetry transformations used to generate equivalent atoms: #1 $-x+2$, y, $-z+1$; #2 $x+1/2$, $y+1/2$, z; #3 $-x+3/2$, $y+1/2$, $-z+2$; #4 $-x+2$, y, $-z+2$; #5 $x-1/2$, $y-1/2$, z.

the dielectric permittivity ε_{rc} along the *c* axis sharply increases to reach a value range of ε_{rc}(**1**) ≈2021–2167 with increasing temperature. Thus, the dielectric anisotropy of $\Phi\varepsilon=\varepsilon_{rc}/\varepsilon_{ra}$ can be estimated to be about 140. Similarly, the dielectric permittivity ε_{rb} along the *b* axis also sharply increases to reach a maximal value range, among the three crystallographic axes, of ε_{rb}(**1**) ≈2121–2266 with increasing temperature . The dielectric anisotropy of $\Phi\varepsilon=\varepsilon_{rb}/\varepsilon_{ra}$ is estimated to reach a maximal value of 147 (Figure 2). To our knowledge, such giant dielectric anisotropy is unprecedented and this value remains constant or temperature-independent with respect to the reported maximal dielectric anisotropy of 70–90, which sharply drops to a normal value or vanishes beyond the phase-transition temperature.[6] In addition, the temperature-independent dielectric behavior is similar to that found in other metal-organic frameworks,[7] non-deuterated organic solid acids,[8] and a homochiral trinuclear Ni^{II} molecule with a dielectric anisotropy of maximal 3.47 due to its non-laminar structural features.[4c]

As mentioned earlier, laminar compounds in principle display the largest anisotropy due to their structural nature. Layered MOF **1** abides by this rule; when *E* is parallel to the $[Eu(Lig)_2(X_2O)_2]^+$ (X = H or D) ionic layer , as depicted in Figure 1 (right-hand side), the dipolar moment along the *b* and *c* axes are larger, which leads to a extremely large dielectric response along the two directions. On the other hand, when *E* is perpendicular to the $[Eu(Lig)_2(X_2O)_2]^+$ (X = H or D) ion layer, as shown in Figure 1 (bottom left), the dielectric constant is much smallest among the three axes, probably due to the layers in this direction composed of multi-layers anionic capacitors that are almost too fixed to move, leading to the smallest dielectric response.

To confirm such giant dielectric anisotropy existing in MOF **1**, the dielectric permittivities of the deuterated MOF **2** along the three crystallographic axes was measured (Figure 3). The dielectric permittivity along the *a* axis is also the smallest, reaching a value range of ε_{ra}(**2**) ≈22.4–23.7. This allowed the deuterated effect {defined as $[\varepsilon_{ra}(\mathbf{2})-\varepsilon_{ra}(\mathbf{1})]/\varepsilon_{ra}(\mathbf{1})$} to be estimated to be in the range of 54–57% enhancement. However, the deuterated effect along other two crystallographic axes essentially vanished. Despite this, the dielectric constants of MOF **2** along the *c* and *b* axes are still slightly larger than those of MOF **1** along these axes, reaching ε_{rc}(**2**) ≈2259–2397 and ε_{rb}(**2**) ≈2317–2383, respectively.

On the basis of the above results, it suggests that H−(D−) bonds between H_2O and the ClO_4^- ion are very strong

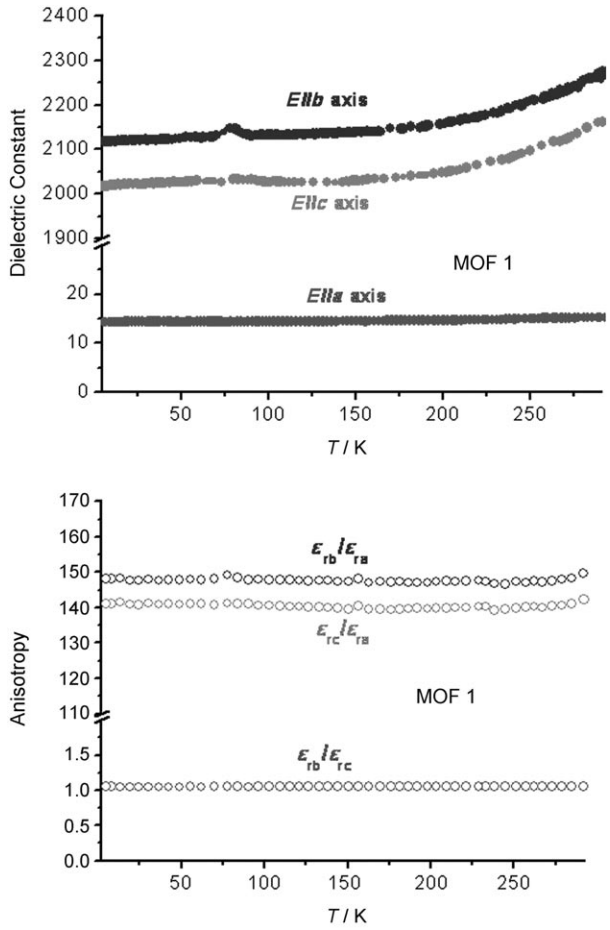

Figure 2. Top: Permittivity (ε_r) of MOF **1** as a function of temperature upon application of E approximately parallel to the a, b, and c crystal axes directions. The measurements were made at a high frequency of 1 MHz. Bottom: Anisotropic ratio as a function temperature.

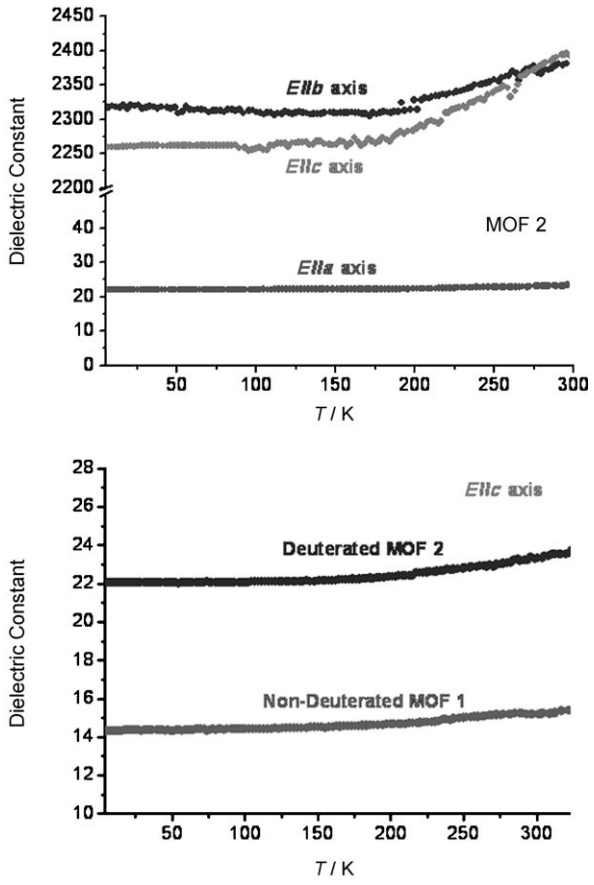

Figure 3. Top: Permittivity (ε_r) of **2** with temperature upon application of E approximately parallel to the a, b, and c crystal axes directions. The measurements were made at a high frequency of 1 MHz. Bottom: Isotopic effect [(22.11–14.35)/14.35 = 54 %] along the a axis.

along the a axis and this feature results in the formation of a larger deuterated effect taking place when two H_2O molecules are replaced by two D_2O molecules.[9] The dielectric anisotropies ($\Phi\varepsilon = \varepsilon_{rb}(\mathbf{2})/\varepsilon_{ra}(\mathbf{2})$ and $\Phi\varepsilon = \varepsilon_{rc}(\mathbf{2})/\varepsilon_{ra}(\mathbf{2})$) of MOF **2** still exceed 100, although they are slightly smaller than that of MOF **1**. Thus, laminar homochiral Eu–MOF reported in this work exhibits unprecedented huge and stable dielectric anisotropy.

According to the Claussius–Mossotti equation, $[(\varepsilon_r-1)/(\varepsilon_r+2)] = 4\pi N_A\beta\rho/3M$ in which N_A, β, ρ, and M are Avogadro's number, molecular polarizability, density, and molecular weight, respectively. Generally, ε_r of MOF **2** should be slightly larger than that of MOF **1** after deuteration according to this rule. Furthermore, as giant dielectric anisotropy may come from molecular polarizability anisotropy, the dielectric constant ε_r along different crystallographic directions should be written as $[(2C\beta+1)/(1-C\beta)]$ according to the Claussius–Mossotti equation in which C $(=4\pi N_A\rho/3M)$ is a constant. Since β is a vector in a crystal, β_{ij} should be written as:

$$\begin{pmatrix} \beta_{11} & \beta_{12} & \beta_{13} \\ \beta_{21} & \beta_{22} & \beta_{23} \\ \beta_{31} & \beta_{32} & \beta_{33} \end{pmatrix}$$

The dielectric vector $\varepsilon_{rij} = [(2C\beta_{ij}+1)/(1-C\beta_{ij})]$. The molecular polarizability (β_{11}) when E is parallel to the a axis is much smaller than those of β_{22} and β_{33} (E parallel to the b and c axes), probably due to E being perpendicular to the layer of $[Eu(Lig)_2(X_2O)_2]^+$, as this layer has larger shielding effect to E resulting in the smallest polarizability. However, the $[Eu(Lig)_2(X_2O)_2]^+$ layer is parallel to E along b and c axes and the ionic polarizability of ClO_4^- and $[Eu(Lig)_2(X_2O)_2]^+$ reach a maximum values, leading to the sharp increase of β_{22} and β_{33}. Thus, the observed dielectric response should obey the order $\varepsilon_{rc} \approx \varepsilon_{rb} \gg \varepsilon_{ra}$.

In addition, the giant dielectric anisotropy should be associated with a strong ferroelectric property. Figure 4 clearly shows that there is an electric hysteresis loop that is a typical ferroelectric feature with a remnant polarization (P_r) of approximately 0.025 $\mu C cm^{-2}$ and coercive field (E_c) of around 0.15 $kV cm^{-1}$. The saturation spontaneous polarization (P_s) of **1** is about 0.1 $\mu C cm^{-2}$, which is smaller than that typical for ferroelectric materials, for example, KH_2PO_4 ($P_s = 5.0\ \mu C cm^{-2}$) and triglycine sulfate ($P_s = 3.0\ \mu C cm^{-2}$), but still smaller than that of $NaKC_4H_4O_6{\cdot}4H_2O$ (Rosal salt, $P_s = 0.25\ \mu C cm^{-2}$). Figure 4 (bottom) also clearly shows that there is an electric hysteresis loop, which is a typical ferro-

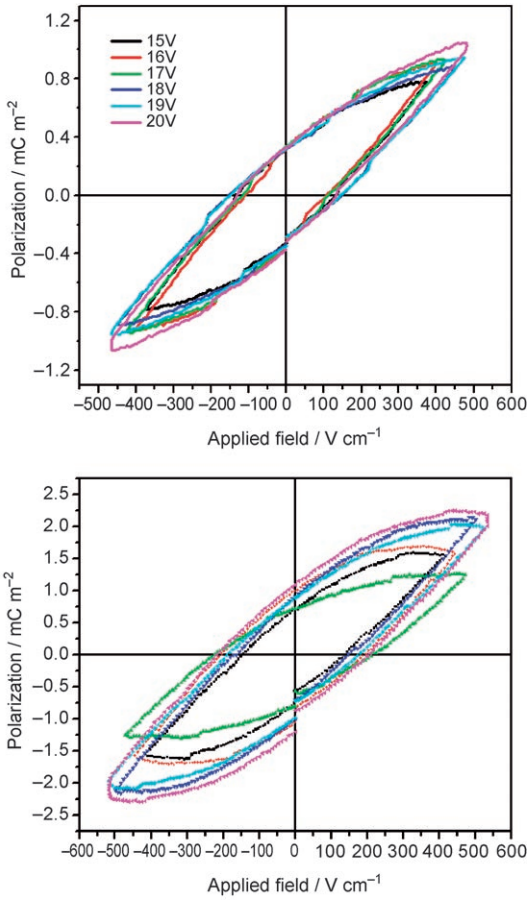

Figure 4. An electric hysteresis loop of a pellet of powders of MOF **1** (top) and **2** (bottom) was observed with an RT66 ferroelectric tester at room temperature.

electric feature with a P_r of about 0.09 μC cm^{-2} and an E_c of around 0.24 kV cm^{-1}. The P_s of **2** is approximately 0.203 μC cm^{-2}. Thus, deuteration effect of P_r and P_s should be 3.6 and 2.03 times than that of non-deuterated MOF **1**, respectively. Thus, the ferroelectric features further confirm the giant permittivity and dielectric anisotropy.

In conclusion, the present work provides an insight in the search for high dielectric anisotropy; from structure to function by crystal engineering design. In generally, the laminar and homochiral MOF will display larger permittivity anisotropy.

Experimental Section

Synthesis of 1: The hydrothermal reaction of L-ethyl lactate (1.0 mL) in the presence of $Eu(ClO_4)_3{\cdot}6H_2O$ (1 mmol) and water (1.5 mL) sealed Pyrex tube at 110 °C for 2–4 days gave colorless block compound **1** in 50% yield based on $Eu(ClO_4)_3{\cdot}6H_2O$ after cooling down. IR: $\tilde{\nu}$ = 3480 (brs), 2980 (vw), 2937 (vw), 1603 (vs), 1470 (m), 1434 (m), 1359 (m), 1315 (w), 1241 (w), 1105 (vs), 933 (w), 870 (w), 781 (w), 628 (w), 570 (w), 452 cm^{-1} (w); elemental analysis calcd (%) for $C_6H_{14}ClO_{12}Eu$: C 15.46, H 3.01; found: C 15.38, H 3.04.

Synthesis of 2: The deuteratothermal reaction of L-ethyl lactate (1.0 mL) in the presence of $Eu(ClO_4)_3{\cdot}6H_2O$ (1 mmol) and deuterated oxide (D_2O; 1.5 mL) sealed Pyrex tube at 110 °C for 2–4 days gave colorless block compound **2** in 45% yield based on $Eu(ClO_4)_3{\cdot}6H_2O$ after cooling down. IR: $\tilde{\nu}$ = 3466 (brs), 2980 (vw), 2937 (vw), 2515 (m), 1602 (vs), 1465 (m), 1433 (m), 1358 (m), 1313 (w), 1241 (w), 1107 (vs), 934 (w), 868 (w), 777 (w), 628 (w), 567 (w), 451 cm^{-1} (w); elemental analysis calcd (%) for $C_6H_{10}D_4ClO_{12}Eu$: C 15.33, H 2.13; found: C 15.28, H 2.08.

Acknowledgements

This work is supported by 973 (2006CB806104), a Distinguished Young Scholar Fund to R.-G. Xiong. (No.20225103), and the National Natural Science Foundation of China.

[1] D. Marchand, C. Fretigny, C. M. Lagues, A. P. Legrand, E. McRae, J. F. Mareche, M. Lelaurain, *Carbon* **1984**, *22*, 497.
[2] H. Korner, A. Shiota, T. J. Bunning, C. K. Ober, *Science* **1996**, *272*, 252.
[3] Y.-I. Kim, W. Si, P. M. Woodward, E. Sutter, S. Park, T. Vogt, *Chem. Mater.* **2007**, *19*, 618.
[4] a) R.-G. Xiong, X. Xue, H. Zhao, X.-Z. You, B. F. Abrahams, Z. Xue, *Angew. Chem.* **2002**, *114*, 3954; *Angew. Chem. Int. Ed.* **2002**, *41*, 3800; b) Q. Ye, Y.-M. Song, G.-X. Wang, D.-W. Fu, K. Chen, P. W. H. Chan, J.-S. Zhu, D. S. Huang, R.-G. Xiong, *J. Am. Chem. Soc.* **2006**, *128*, 6554; c) D.-W. Fu, Y.-M. Song, G.-X. Wang, Q. Ye, R.-G. Xiong, T. Akutagawa, T. Nakamura, P. W. H. Chan, S. D. Huang, *J. Am. Chem. Soc.* **2007**, *129*, 5346; Q. Ye, H. Zhao, Z.-R. Qu, D.-W. Fu, R.-G. Xiong, Y.-P. Cui, T. Akutagawa, P. W. H. Chan, T. Nakamura, *Angew. Chem.* **2007**, *119*, 6976; *Angew. Chem. Int. Ed.* **2007**, *46*, 6852.
[5] Crystal data of **1**, $C_6H_{14}ClO_{12}Eu$, M_r = 465.58, monoclinic, C_2, a = 8.6786(6), b = 8.3965(6), c = 10.2153(7) Å, β = 92.040(1)°, V = 743.92(9) Å^3, Z = 2, ρ_{calcd} = 2.079 Mg m^{-3}, R_1 = 0.0508, wR_2 = 0.1239, μ = 4.448 mm^{-1}, S = 1.043; Flack = 0.04(5). Crystal data **2**: $C_6H_{10}D_4ClO_{12}Eu$, M_r = 469.61, monoclinic, C_2, a = 8.689(2), b = 8.410(2), c = 10.224(3) Å, β = 92.057(4)°, V = 746.7(3) Å^3, Z = 2, ρ_{calcd} = 2.089 Mg m^{-3}, R_1 = 0.0465, wR_2 = 0.1150, μ = 4.432 mm^{-1}, S = 1.058; Flack = 0.02(5). The structures were solved with direct methods by using the program SHELXTL (Sheldrick, 1997).[10] All non-hydrogen atoms were located from the trial structure and refined anisotropically with SHELXTL by using full-matrix least-squares procedures. The hydrogen and deuterium atom positions were fixed geometrically at calculated distances and allowed to ride on the parent carbon atoms. The final difference Fourier map was found to be featureless. CCDC 651944 (**1**) and 651945 (**2**) contain the supplementary crystallographic data for this paper. These data can be obtained free of charge from The Cambridge Crystallographic Data Centre via www.ccdc.cam.ac.uk/data_request/cif.
[6] S. Horiuchi, F. Ishii, R. Kumai, Y. Okimoto, H. Tachibana, N. Nagaosa, Y. Tokura, *Nat. Mater.* **2005**, *4*, 163.
[7] H.-B. Cui, Z. Wang, K. Takahashi, Y. Okano, H. Kobayashi, A. Kobayashi, *J. Am. Chem. Soc.* **2006**, *128*,15074.
[8] I. Takasu, A. Izuka, T. Sugawara, T. Mochida, *J. Phys. Chem. A J. Phys. Chem. B J. Phys. Chem. A J. Phys. Chem. B* **2004**, *108*, 5527.
[9] T. Akutagawa, S. Takeda, T. Hasegawa, T. Nakamura, *J. Am. Chem. Soc.* **2004**, *126*, 291.
[10] G. M. Sheldrick, SHELXTL V5.1 Software Reference Manual, Bruker AXS, Inc., Madison, Wisconsin (USA), **1997**.

Received: September 13, 2007
Published online: February 12, 2008

